Volume 1 | Number 1 | Jan 2013 | Pages 1–100

Dalton Transactions

An international journal of inorganic chemistry
www.rsc.org/dalton

ROYAL SOCIETY OF CHEMISTRY

ROYAL SOCIETY OF CHEMISTRY

www.rsc.org/dalton

Enhancing upconversion luminescence of NaYF$_4$:Yb/Er nanocrystals by Mo^{3+} doping and their application in bioimaging

Dongguang Yin[1]*, Chengcheng Wang[1], Juan Ouyang[1], Kailin Song[1], Bing Liu[1], Xianzhang Cao[1], Lu Zhang[1], Yanlin Han[1], Xie Long[2]*, Minghong Wu[1]*

[1]*School of Environmental and Chemical Engineering, Shanghai University, Shanghai 200444, China*

[2] *Yueyang Hospital of Integrated Traditional Chinese and Western Medicine, Shanghai 200437, China*

*Corresponding author: ydg@shu.edu.cn

Abstract

Enhancement of upconversion luminescence is imperative for the applications of upconversion nancrystals (UCNs). In this work, we investigated the upconversion luminescence enhancement of NaYF$_4$:Yb/Er by Mo^{3+} ions doping. It was found that the upconversion luminescence intensities of green and red lights of the UCNs co-doped with 10 mol% Mo^{3+} ions were enhanced by 6 and 8 times, respectively. This enhancement offers a potential increase in overall upconversion nanocrystals detectability. The HeLa cells imaging using NaYF$_4$:Yb/Er/Mo as luminescent probe showed bright upconversion fluorescence. Moreover, the Mo^{3+} doping made the UCNs presenting excellent paramagnetic behavior. It is expected that the as-prepared UCNs with a high upconversion luminescence and excellent paramagnetic properties are promising bi-functional nanoprobes for sensitive multi-modality bioimaging and other optical applications.

1. Introduction

In recent years, lanthanide-doped UCNs, especially inherent low phonon energy $NaYF_4$-based systems, have drawn considerable attention due to their unique optical properties and potential applications such as vivo and vitro imaginges, volumetric displays and solar cells.[1-8] However, the applications of these UCNs are still constrained due to their low upconversion luminescent (UCL) efficiency. Thus improvement of UCL is imperative for the applications of the UCNs. Up to date, various attempts have been devoted to improve the UCL of UCNs, such as doping with different rare earth ions,[9-13] varying the crystal phase of the nanocrystals,[14-17] fabricating core-shell structure,[18-22] utilizing metal-enhanced fluorescence.[23-28]

It is well-known that the upconversion luminescence of lanthanide ions-doped nanocrystals is dependent on their intra 4f transition probabilities, which is remarkable affected by the local crystal field of the lanthanide ions.[29] Consequently, fine-tuning the local crystal of the lanthanide ions is an effective strategy to increase the UCL of lanthanide ions-doped nanocrystals.[30] For example, Huang et al. observed enhanced-upconversion emissions in hexagonal $NaYF_4$ when it was tri-doped with $Sc^{3+}/Er^{3+}/Yb^{3+}$.[13] Zhao et al. found that the UCL intensities of 452nm and 479nm of the $NaYF_4$:Yb/Tm co-doped with 7 mol% Li^+ ions were increased by 8 and 5 times, respectively.[31] Most recently, it has been reported that the visible green and red UCLs in Er^{3+}/Yb^{3+} doped β-$NaGdF_4$ nanocrystals are greatly enhanced by tri-doping with Fe^{3+} ions.[30] These UCL enhancements can be attributed to the altering of crystal field symmetry arisen from the co-doped ions.[29-31] Inspired by these, we investigated the UCL enhancement of $NaYF_4$:Yb/Er by tri-doping with Mo^{3+} ions in this study. It is found

that this approach can tune and enhance the UCL of the UCNs. Moreover, the doped-Mo^{3+}

ions can make the nanocrystals presenting excellent paramagnetic behavior. To the best of our

knowledge, this is the first time to tune the UCL and magnetic properties of UCNs by Mo^{3+}

doping. It is expected that the as-prepared UCNs with a higher UCL and excellent

paramagnetic properties is a promising bi-functional nanoprobe for multi-modality

bioimaging and other optical applications.

2. Experimental

2.1. Materials

Rare earth oxides Y_2O_3 (99.999%), Yb_2O_3 (99.999%), and Er_2O_3 (99.999%) were purchased

from Shanghai Yuelong New Materials Co. Ltd. Oleic acid (OA) (>90%)，1-octadecene

(>90%) and $MoCl_3$ were purchased from Sigma-Aldrich. NaOH, NH_4F, sodium citrate,

hydrochloric acid, ethanol, methanol and cyclohexane were supplied from Sinopharm

Chemical Reagent Co., Ltd. (Shanghai). $LnCl_3$ (Ln:Y, Yb, Er) were prepared by dissolving the

corresponding metal oxides in hydrochloric acid at elevated temperature.

2.2. Synthesis of NaYF₄:Yb/Er/Mo upconversion nanocrystals

$NaYF_4$ UCNs doped with Yb^{3+}, Er^{3+} (18, 2 mol%) and Mo^{3+} ions (0, 5, 10, 15 and 20 mol%)

were synthesized following a reported procedure with some modification, using oleic acid as

the coordinating ligand and 1-octadecene as the non-coordinating solvent.[32,33] In the case of

NaYF$_4$:Yb/Er/Mo (18, 2, 10 mol%) nanocrystals, 0.70 mmol of YCl$_3$, 0.18 mmol of YbCl$_3$, 0.02 mmol of ErCl$_3$, 0.1 mmol of MoCl$_3$, 15 mL of octadecene and 6 mL of oleic acid (OA) were added to a 100 mL 3-necked flask. The flask was then heated to 170 ºC under a vacuum and held at this temperature for 60 min to get a homogeneous solution. Subsequently, the flask was cooled down to room temperature and then 10 mL methanol solution containing 4 mmol NH$_4$F and 2.5 mmol NaOH was dropwise added into the flask. The resulting solution was stirred at room temperature for 30min and then heated slowly to 110 ºC to evaporate methanol. The reaction vessel was heated up to 305 ºC under nitrogen atmosphere and kept at this temperature for 1 h. After the flask was cooled down to room temperature, the UCNs were precipitated by adding ethanol (15 mL), then centrifuged and washed with ethanol. The isolated OA-stabilized UCNs were stored in cyclohexane. In other cases of synthesis of NaYF$_4$:Yb/Er/Mo (18, 2, x mol%), where x=0, 5, 15 and 20% mol%, the synthetic procedures were similar to that of NaYF$_4$:Yb/Er/Mo (18, 2, 10 mol%), except change the amounts of YCl$_3$ and MoCl$_3$.

2.3. Synthesis of hydrophilic sodium citrate-coated NaYF$_4$:Yb/Er/Mo upconversion nanocrystals

The above prepared UCNs in oleic acid are hydrophobic which can only be dispersed in non-polar solvents. In order to perform its biomedical application, it should be transformed to hydrophilic. In this study, a ligand exchange method was used for rendering these UCNs dispersible in water.[34,35] A typical procedure is as follow: NaYF$_4$:Yb/Er/10%Mo UCNs (20mg) dissolved in 6 mL of cyclohexane and sodium citrate (2 mmol) dissolved in 10 mL of

deionized water were mixed and stirred for 3 h. Then cyclohexane was removed by separator. The obtained citrate-coated UCNs (Cit-NaYF$_4$:Yb/Er/10%Mo) were isolated by centrifugation, washed several times with deionized water, and then redispersed in deionized water to form a transparent solution.

2.4. Characterization

X-ray powder diffraction (XRD) patterns of the several nanocrastals were performed on a Rigaku D/max-2500 X-ray diffractometer at a scanning rate of 8°/min in the 2θ range from 10 to 70° using Cu Kα radiation. Transmission electron microscopy (TEM) analyses were taken on a JEOL JEM-2010F electron microscope operating at an accelerating voltage of 200 kV. TEM specimens were prepared by placing a drop of diluted cyclohexane dispersion containing samples on the surface of a carbon-coated copper grid. Energy-dispersive X-ray analysis (EDX) of the samples was performed during high-resolution transmission electron microscopy (HRTEM) measurements to obtain the elements of samples. Inductively Coupled Plasma-Atomic Emission Spectrometry (ICP-AES) were measured on PERKINE 7300DV spectrograph. The upconversion luminescence emission spectra were recorded with an Edinburgh LFS-920 fluorescence spectrometer by using an external 0-3W adjustable laser (980 nm, Beijing Hi-Tech Optoelectronic Co., China) as the excitation source. The magnetization as a function of the applied magnetism of the NaYF$_4$-based nanocrystals was recorded using a Lake-shore 7407 vibrating sample magnetometer.

2.5 Cell Cytotoxicity assay

Cell vaiablity was measured using a 3-(4,5-dimethylthiazol-2-yl)-2,5,-diphenyltetrazolium bromide (MTT) proliferation assay.[36,37] Briefly, HeLa cells were seeded in a in a 96-well flat-bottomed microplate (2×10^4 cells per well) and cultured in 100 μL growth medium at 37 ºC and 5% CO_2 for 12 h. Cell culture medium in each well was then replaced by 100 μL cell growth medium, containing Cit-NaYF$_4$:Yb/Er/10%Mo with concentrations ranging from 100 to 1000 μg/mL. After incubation for 24 h, 100 μL MTT (0.5 mg/mL in PBS solution) was added to each well for further 4 h incubation at 37 ºC. The growth medium was removed gently by suction, and 150 μL DMSO was then added to every well as solubilizing agent, sitting at room temperature for 2 h. The absorbance at the wavelength of 490 nm was measured by a Microplate Reader (BIO-RAD Corporation), and each data point was represented as mean ± standard deviation (SD) from sextuplicate wells.

2.6. Cell imaging

The confocal UCL imaging of HeLa Cells with the prepared UCNs was carried out as previous reported literature.[36,37] In typically, the HeLa cells were grown in MEM (Modified Eagle's Medium) supplemented with 10% PBS (Fetal Bovine Serum) at 37 ºC and 5% CO_2. Cells (5×10^8/L) were plated on 14 mm glass coverslips and allowed to adhere for 24 h. Before the experiments, HeLa cells were washed with PBS buffer (pH = 7) and then incubated with 200 μg/mL Cit-NaYF4:Yb/Er/10%Mo at 37 ºC for 5 h. Cells imaging was performed with a laser scanning upconversion luminescence microscope.

3. Results and discussions

3.1. Crystalline phase and morphology of the nanocrystals

Fig. 1 shows the XRD pattern of $NaYF_4$ nanocrystals doped with 18 mol% Yb^{3+}, 2 mol% Er^{3+} ions and 0-20 mol% of Mo^{3+} ions. All the diffraction peaks can be indexed to the hexagonal β-$NaYF_4$ (JCPDS file number 16-0334). No other impurity peaks were detected, which revealed that pureβ-$NaYF_4$ had been fatricated. This indicates that the Mo^{3+} doping has no influence on the crystalline phase of the nanocrystals. The enlarged area of main diffraction peak (201) shows that the diffraction peak shifts towards larger angles as the concentration of Mo^{3+} ions increase up to 5 mol%, and moves in reverse for Mo^{3+} ion concentrations of 5–20 mol%. The peak shifting indicates that Mo^{3+} ions can be doped into the host lattice through the substitution or occupation of the interstitial below 20 mol%. This result is similar to the reported Li^+ ions doping.[29]
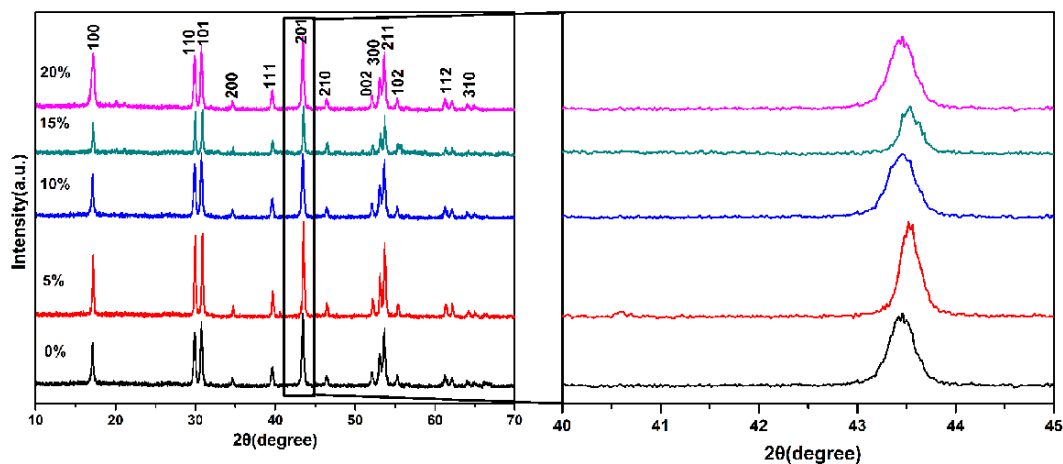
Fig. 1 XRD patterns of $NaYF_4$ nanocrystals doped with Mo^{3+} at different concentrations

The TEM images of the prepared nanocrystals are shown in Fig. 2. It is found that the grain

size of the UCNs increases with increase in the doped-Mo^{3+} content. With increase in Mo^{3+}

contents from 0% to 5%, 10%, 15% and 20%, the average grain sizes of the UCNs are 34, 39,

59, 92 and 109nm, respectively. The size evolution of the nanocrystals may be attributed to

the strong impact of the Mo^{3+} ions on crystal growth rate through surface charge modification,

which are similar to the cases where Gd^{3+} or Mn^{2+} ions were doped in the nanocrystals.[15,38]

The real mechanism is not very clarity, needing to be further investigated in our following

work.

Fig. 2f shows the typical HRTEM image of $NaYF_4$:18%Yb/2%Er/10%Mo with *d*-spacing

of 0.52nm, corresponding to the (100) lattice plane of the hexagonal phase $NaYF_4$. Fig. 2g

shows the EDX pattern of $NaYF_4$:18%Yb/2%Er/10%Mo. As can be seen in Fig. 2g, almost

all of the elements including Y, Yb, Mo, Na, F can be detected, confirming the Mo^{3+} ions

were successfully doped in the UCNs. The actual concentration of Mo^{3+}ions within the UCNs

was checked by ICP-AES. The measured mass percentage of Mo^{3+} ions existed in the

materials is 1.31%, 2.04%, 3.60%, 5.00% respectively, corresponding to the stoichiometric

mol percentage of Mo^{3+} ions of 5%, 10%, 15%, 20% and stoichiometric mass percentage of

2.66%, 5.50%, 8.65%, 11.5%, respectively. The measured values are lower than that of

theoretical values, indicating that a part of Mo^{3+} ions is lost during the doping process.
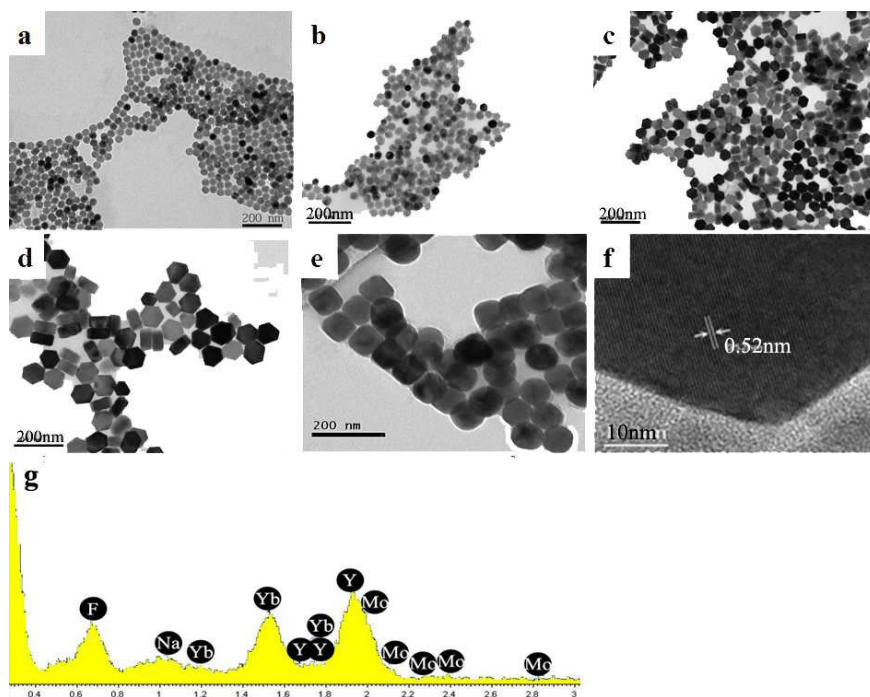
Fig. 2 TEM images of the NaYF$_4$:18%Yb/2%Er/X%Mo nanocrystals: x= 0% (a), 5% (b), 10% (c), 15% (d) and 20% (e); (f) high-resolution TEM imagine of the UCNs shown in (c); (g) Energy-dispersive X-ray analysis (EDXA) patterns of NaYF$_4$:18%Yb/2%Er/10%Mo.

3.2. Upconversion luminescence properties of the nanocrystals

Fig. 3 shows the upconversion emission spectra of NaYF$_4$:Yb/Er (18, 2 mol%) nanocrystals doped with different concentrations of Mo^{3+} ions under 980 nm laser excitation. All the nanocrystals exhibited three distinct bands in the range of 475-700 nm. Two green emissions bands concentrated from 512 to 535 nm and from 535 to 556 nm were attributed to the ^{2}H$_{11/2}$ / ^{4}I$_{15/2}$ and ^{4}S$_{3/2}$ / ^{4}I$_{15/2}$ transitions of Er^{3+}, respectively. The red emission from 640 to 670 nm was due to the ^{4}F$_{9/2}$ /^{4}I$_{15/2}$ transition of Er^{3+}.[39]

Obviously, the UCL intensities were drastically changed when the Mo^{3+} ions were doped in the nanocrystals, and the Mo^{3+} ions concentrations had a huge effect on the UCL intensities. The upconversion emission intensities in both the green and red regions distinctly increased

when the concentration of Mo^{3+} ions increased from 0 to 10 mol%, but subsequently

decreased with increase in the concentration over 10 mol%. The strongest UCL was observed

in the sample with Mo^{3+} concentrations of 10 mol%. The inset of Fig. 3 shows the

enhancement of green and red upconversion emissions as a function of Mo^{3+} concentration.

The green and red emission intensities were measured to be about 6 and 8 times that of the

Mo^{3+}-absent sample, respectively.

It is well known that the upconversion luminescence intensities of Er^{3+}-doped UCNs are

dependent on their 4f transition probabilities which is affected significantly by the local

crystal field symmetry of the Er^{3+}, and a hypersensitive transition can be produced by

changing the environment of Er^{3+}.[29,40] The doping of $NaYF_4$:Yb/Er NPs with small radius

Mo^{3+} ions would tailor the surrounding environment around the Er^{3+} ions in the crystal field.

In the $NaYF_4$ host lattice, the Mo^{3+} ions exist by substituting the Y^{3+} site due to the same

charge value. Substituting the Y^{3+} ions with the small Mo^{3+} ions can cause the host lattice to

shrink, which results in the decrease of cell volume. This will lead to a decrease of the

average F^{-1}–Ln^{3+} bond lengths and breaking of the local crystal field symmetry around the

lanthanide ions.[29,31,41] The asymmetric surrounding environment of lanthanide ions favors the

hypersensitive transitions, subsequently increasing the upconversion luminescence.[40]

However, when the Mo^{3+} concentration increased from 10 mol% to 20 mol% both green and

red emissions became weak. This can be assumed that superfluous dopant induces significant

distortion to the lattice, which affect the spatial distribution of the lanthanide ions, induce a

concentration quenching and reduce the emission intensity.[31] This phenomena of initial

enhancement and subsequent decrease of upconversion emission intensity were also observed

in the UCNs co-doped with Li^+ and Fe^{3+}. [29, 30]
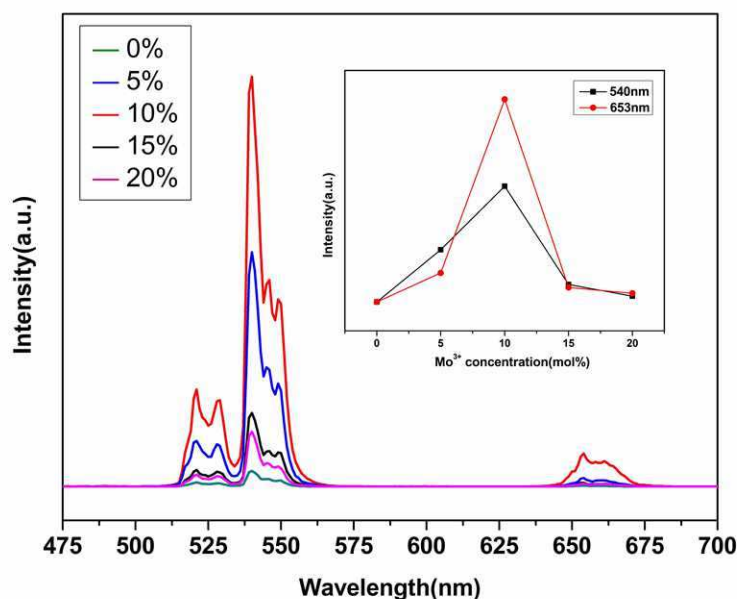
Fig. 3 Upconversion luminescence spectra of the prepared nanocrystals

The above mentioned UCNs were prepared with different sizes. Considering the size of the UCNs probably affects the UCL intensity, we synthesized another batch of same sized UCNs with doping different amount of Mo^{3+} ions through modifying the reaction condition. For synthesizing the same sized UCNs doped with 0, 5, 10, 15, 20% mol Mo^{3+}, the synthetic method and procedure were similar to the above different sized UCNs but with modification reaction time of 1.5, 1.5, 1, 1.5, 1.5 respectively, and the reaction temperature of 315, 313, 305, 308, 302 respectively. As shown in Fig. 4(I), all the prepared new batch of UCNs displays plate-liked structure with diameter of 58±5nm. It can be seen from Fig.4 (II) that their UCL properties are similar to that of the different sized UCNs. The strongest UC emission is also observed in the sample containing 10mol% Mo^{3+}. The green and red emissions are 5 and 7 times higher than that of Mo^{3+}-free sample, respectively. These results demonstrate that the enhancement of the UCL can be dominantly attributed to the doping of Mo^{3+}, while the influence of size of the UCNs is negligible.

11
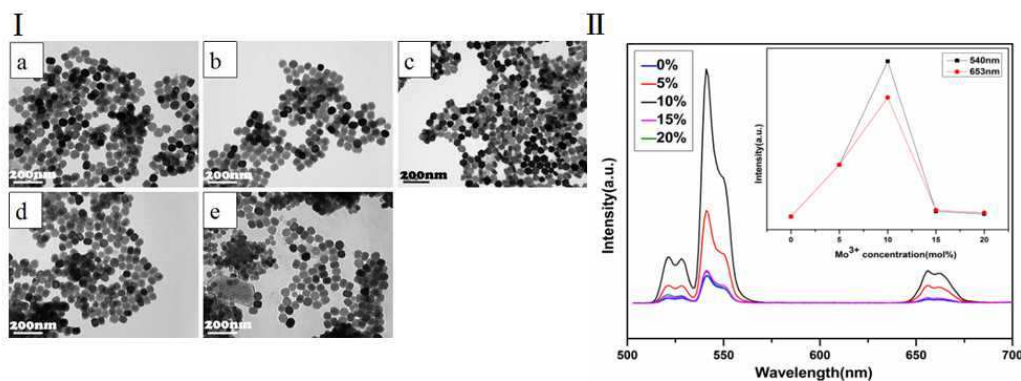
Fig. 4 TEM images (I) of the NaYF$_4$:18%Yb/2%Er/X%Mo nanocrystals: x= 0% (a), 5% (b), 10% (c), 15% (d), 20%, and upconversion luminescence spectra(II) of the same sized UCNs.

Besides the excellent upconversion luminescence, the Mo^{3+}-doped NaYF$_4$ nanocrystals also present particular magnetic properties due to the large magnetic moment of Mo^{3+}. Fig. 5 shows the magnetization as a function of an applied magnetic field (from -18 kOe to 18 kOe) for NaYF$_4$ nanocrystals doped with different amount of Mo^{3+}, demonstrating that all of the samples present typical paramagnetic behavior. The magnetization of the NaYF$_4$ nanocrystals can be modified from 0.06 emu g^{-1} to 0.48 emu g^{-1} at 18 kOe with increasing the Mo^{3+} doping content from 0% to 20%. The paramagnetic behavior could be mainly assigned to the role of unpaired inner electrons.[14,42] Owing to the Mo^{3+} having three unpaired 4d electrons which are bounded to the nucleus, thus the Mo^{3+} has a higher magnetic moment and induce the nanocrystals exhibiting paramagnetic behavior. The presence of paramagnetic behavior indicates that the nanocrystals have potential applications in magnetic resonance imaging and bio-separation.
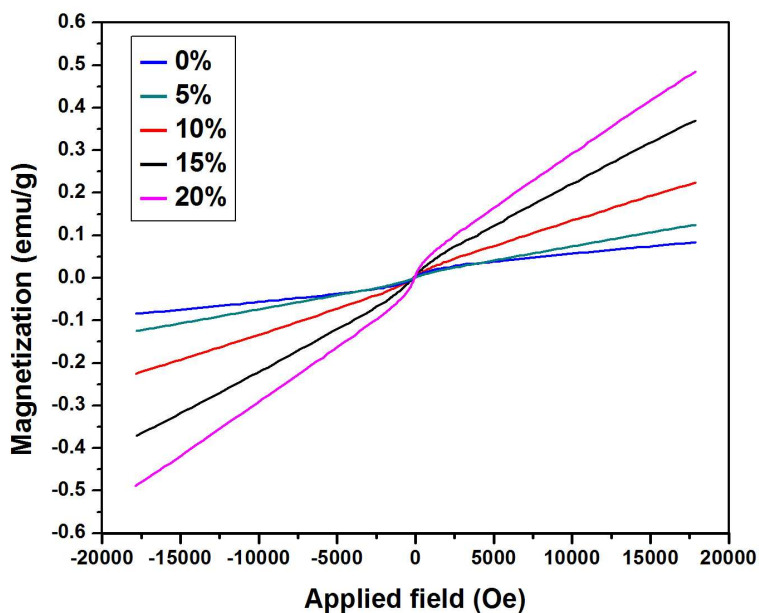
Fig.5 The magnetic hysteresis loops at 300 K of the prepared nanocrystals

3.3. Cytotoxicity test

Toxicity is a critical factor determining the feasibility of the as-prepared UCNs in bioimaging

applications. The viability of HeLa cells after exposure to UCNs with different concentrations

was measured by a standard MTT assay. As shown in Fig. 6, the prepared UCNs

(NaYF$_4$:Yb/Er/10%Mo) showed negligible cytotoxicity toward HeLa cells, even at a high

dosage of 1000 μg/mL for 24 h (viability > 87%). The high viability of cells demonstrates the

good biocompatibility and the potentiality of the UCNs for bioimaging applications.[43, 44]
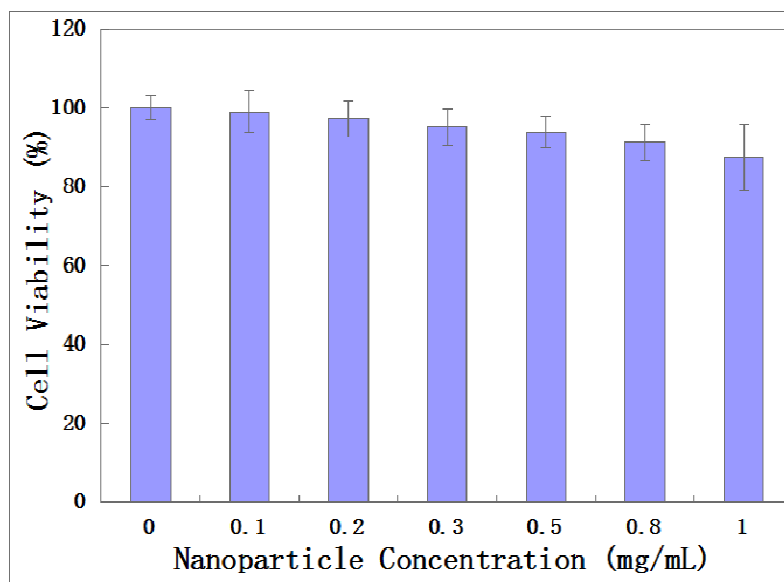
Fig. 6 Cell viability data of Hela cells after incubation with the Cit-NaYF$_4$:Yb/Er/10%Mo

with different concentrations for 24 h

3.4. The application of UCL imaging of living cells in vitro

The cellular uptake of the Cit-NaYF$_4$:Yb/Er/10%Mo were carried out by incubating HeLa

cells with 200 μg/mL Cit-NaYF$_4$:Yb/Er/10%Mo in PBS buffer (pH = 7) at 37 ℃ for 5 h.

Confocal microscopy images are shown in Fig. 7. As shown in Fig. 7 B and C, strong UCL

signals at 520-560 nm (green light) and 640-680 nm (red light) are detected. It can be seen

from the overlay of confocal luminescence and bright-field images that brightly luminescent

aggregates are visible in the cells, which indicate that the luminescence comes from the HeLa

cells and the Cit-NaYF$_4$:Yb/Er/10%Mo has been internalized into the cells.[45, 46] These results

imply that the Cit-NaYF$_4$:Yb/Er/10%Mo can be utilized as potential upconversion

luminescence probe for bioimaging.
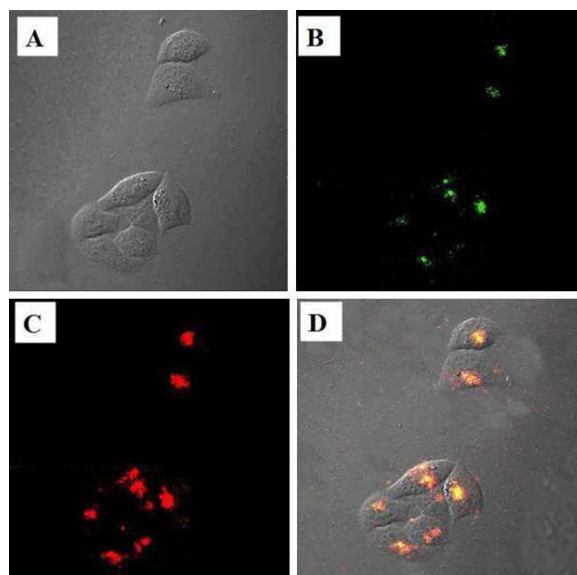
Fig. 7. Bright field image of HeLa cells(A), confocal images of HeLa cells after incubation with Cit-NaYF$_4$:Yb/Er/10%Mo, collected at green (520-560 nm) (B) and red (640-680 nm) channels (C), and the overlay of bright-field image and panels B and C (D)

4. Conclusions

In summary, NaYF$_4$:Yb^{3+}/Er^{3+} UCNs doped with different concentrations of Mo^{3+} ions were synthesized by a facile solvothermal method for the first time. The results show that the UCL of the UCNs can be significantly enhanced through Mo^{3+} ions doping. Visible green and red UCL in NaYF$_4$:Yb^{3+}/Er^{3+} UCNs are enhanced by up to 6 and 8 times by introducing 10 mol% Mo^{3+} ions, respectively. The Mo^{3+}-doped NaYF$_4$ nanocrystals also exhibit paramagnetic behavior at room temperature with magnetization of up to 0.48 emu g^{-1} at 18 kOe, which provides a simple strategy for combining two functions into a single phase material. The enhancement of the luminescent and paramagnetic properties make the UCNs promising materials in future biomedical engineering applications, such as a in versatile imaging tools

for smart detection or diagnosis.

Notes and references

1 E.M. Chan, G. Han, J.D. Goldberg, D.J. Gargas, A.D. Ostrowski, P.J. Schuck, B.E. Cohen, and D.J. Milliron, *Nano Lett.,* 2012, **12**, 3839.

2 J. Shen, G.Y. Chen, T.Y. Ohulchanskyy, S.J. Kesseli, S. Buchholz , Z.P. Li, P.N. Prasad, and G. Han, *small,* 2013, **9**, 3213.

3 G. S. Yi and G. M. Chow, *Adv. Funct. Mater.* 2006, **16**, 2324.

4 Z.J. Gu, L. Yan, G. Tian, S.J. Li, Z.F. Chai, and Y.L. Zhao, *Adv. Mater*. 2013, **25**, 3758.

5 C.J. Lv, W.H. Di, Z.H. Liu, K.Z. Zheng, and W.P. Qin, *Dalton Trans.,* 2014, **43**, 3681.

6 H.S. Mader, P. Kele, S.M. Saleh, and O.S. Wolfbeis, *Curr. Opin. Chem. Biol.,* 2010, **14**, 582.

7 R. Kumar, M. Nyk, T.Y. Ohulchanskyy, C.A. Flask, and P.N. Prasad, *Adv. Funct. Mater*. 2009, **19**, 853.

8 P. Qiu, N. Zhou, H. Chen, C. Zhang, G. Gao, and D.X. Cui, *Nanoscale,* 2013, **5**, 11512.

9 L.L Wang, M. Lan, Z.Y Liu, G.S. Qin, C.F. Wu, X. Wang, W.P. Qin, W. Huang, and L. Huang, *J. Mater. Chem. C*, 2013, **1**, 2485.

10 M.Y. Ding, C.H. Lu, L.H. Cao, J.B. Song, Y. Ni, and Z.Z. Xu, *J Mater Sci*, 2013, **48**, 4989.

11 S. Heer, K. Kompe, H.U. Gudel, and M. Haase, *Adv. Mater*, 2004, **16**, 2102.

12 J. Shen, G.Y. Chen, A.M. Vu, W. Fan, O.S. Bilsel, C.C. Chang, and G. Han, *Adv. Opt.Mater.,* 2013, **1**, 644.

13 Q. Huang, J. Yu, E. Ma, and K. Lin, *J. Phys. Chem. C,* 2010, **114**, 4719.

14 S.J. Zeng, J.J. Xiao, Q.B. Yang, and J.H. Hao, *J. Mater. Chem.,* 2012, **22**, 9870.

15 G. Tian, Z.J. Gu, L.J. Zhou, W.Y. Yin, X.X. Liu, L. Yan, S. Jin, W.L. Ren, G.M. Xing, S.J.

Li, and Y.L. Zhao, *Adv. Mater.,* 2012, **24**, 1226.

16 A. Hischemoeller, J. Nordmann, and P. Ptacek, *J. Biomed. Nanotechnol.,* 2009, **5**, 278.

17 L.Y. Pan, M. He, J.B. Ma, W. Tang, G. Gao, R. He, H.C. Su, and D.X. Cui, *Theranostics* 2013, **3**, 210.

18 W. Shao, G.Y. Chen, J. Damasco, X.L. Wang, A. Kachynski, T.Y. Ohulchanskyy, C.H. Yang, H. Ågren, and P.N. Prasad, *Opt Lett*, 2014, **39**, 1386.

19 G.Y. Chen, J. Shen, T.Y. Ohulchanskyy, N.J. Patel, A. Kutikov, Z.P. Li, J. Song, R.K. Pandey, H. Agren, P.N. Prasad, and G. Han, *ACS Nano*, 2012, **9**, 8280.

20 F. Zhang, R.C. Che, X.M. Li, C. Yao, J.P. Yang, D.K. Shen, P. Hu, W. Li, and D.Y. Zhao, *Nano Lett.,* 2012, **12**, 2852.

21 M.L. Chen, Y. Ma, and M.Y. Li, *Mater. Lett.,* 2014, **114**, 80.

22 Q.H. Zeng, B. Xue, Y.L. Zhang, D. Wang, X.M. Liu, L.P. Tu, H.F. Zhao, X.G. Kong, and H. Zhang, *CrystEngComm*, 2013, **15**, 4765.

23 T. Jiang, Y. Liu, S.S. Liu, N. Liu, and W.P. Qin, *J. Colloid Interf. Sci.*, 2012, **377**, 81.

24 Z.Q. Li, L.M. Wang, Z.Y. Wang, X.H. Liu, and Y.J.Xiong, *J. Phys. Chem. C*, 2011, **115**,3291.

25 P. Kannan, F.A. Rahim, R. Chen, X. Teng, L. Huang, H.D. Sun, and D.H. Kim, *ACS Appl. Mater. Inter.*, 2013, **5**, 3508.

26 M. Saboktakin, X.C. Ye, S.J. Oh, S.H. Hong, A.T. Fafarman, U.K. Chettiar, N. Engheta, C.B. Murray, and C.R. Kagan, *ACS Nano*, 2012, **6**, 8758.

27 P.Y. Yuan, Y.H. Lee, M.K. Gnanasammandhan, Z.P. Guan, Y. Zhang and Q.H. Xu, *Nanoscale*, 2012, **4**, 5132.

28 J. Sun, H.P. Liu, D. Wu, B. Dong, and L.k. Sun, *Mater. Chem. Phys.,* 2013, **137**, 1021.

29 Q. Cheng, J.H. Sui, and W. Cai, *Nanoscale,* 2012, **4**, 779.

30 P. Ramasamy, P. Chandra, S.W. Rhee, and J. Kim, *Nanoscale*, 2013, **5**, 8711.

31 C.Z. Zhao, X.G. Kong, X.M. Liu, L.P. Tu, F. Wu, Y.L. Zhang, K. Liu, Q.H. Zeng, and H. Zhang, *Nanoscale,* 2013, **5**, 8084.

32 D.G. Yin, K.L. Song, J. Ouyang, C.C. Wang, B. Liu, M.H. Wu, *J. Nanosci. Nonotechnol.*, 2013, **13**, 4162.

33 J. Wang, H.W. Song, W. Xu, B. Dong, S. Xu, B.T. Chen, W. Yu, and S. Zhang, *Nanoscale,*

2013, **5**, 3412

34 T.Y. Cao, T.S. Yang, Y Gao, Y. Yang, H. Hu, and F.Y. Li, *Chem. Commun.,* 2010, **13**, 392.

35 Q. Liu, Y. Sun, T.S. Yang, W. Feng. C.G. Li, F.Y. Li, *J. Am. Chem. Soc.,* 2011, **133**, 17122.

36 Q. Ju, D.T. Tu, Y.S. Liu, R.F. Li, H.M. Zhu, J.C. Chen, Z. Chen, M.D. Huang, and X.Y. Chen, *J. Am. Chem.Soc.*, 2012, **134**, 1323.

37 H.T. Wong, M.K. Tsang, C.F. Chan, K.L. Wong, B. Fei, and J.H. Hao, *Nanoscale*, 2013, **5**, 3465.

38 F. Wang, Y. Han, C.S. Lim, Y. Lu, J. Wang, J. Xu, H. Chen, C. Zhang, M. Hong, and X. Liu, *Nature,* 2010, **463**, 1061.

39 D.M. Yang, X.J. Kang, P.A. Ma, Y.L. Dai, Z.Y. Hou, Z.Y. Cheng, C.X. Li, and J. Lin, *Biomaterials*, 2013, **34**, 1601.

40 D. Li, Y. Wang, X. Zhang, H. Dong, L. Liu, G. Shi, and Y. Song, *J. Appl. Phys.*, 2012, **112**, 094701.

41 X. Q. Chen, Z.K. Liu, Q. Sun, M. Ye, and F. P. Wang, *Opt. Commun.,* 2011, **284**, 2046.

42 W. Chiu, P. Khiew, M. Cloke, D. Isa, H. Lim, T. Tan, N. Huang, S. Radiman, R. Abd-Shukor, M.A.A. Hamid, and C.H. Chia, *J. Phys. Chem. C,* 2010, **114**, 8212.

43 L. Zhao, A. Kutikov, J. Shen, C. Duan, J. Song, and G. Han, *Theranostics,* 2013, 3, 249-257.

44 X.J. Zhu, J. Zhou, M. Chen, M. Shi, W. Feng, and F.Y. Li, *Biomaterials,* 2012, **33**, 4618.

45 Y.H. Lou, M.F. Xu, L. Zhang, Z.K. Wang, S. Naka, H. Okada, and L.S. Liao, *Organic Electronics*, 2013, **14**, 2698.

46 W.Y. Yin, L.N. Zhao, L.J. Zhou, Z.J. Gu, X.X. Liu, G. Tian, S. Jin, L. Yan, W.L. Ren, G.M. Xing, and Y.L. Zhao, *Chem. Eur. J,* 2012, **18**, 9239.